Discrete element modeling of self-healing processes in damaged particulate materials

S. Luding[1], A.S.J. Suiker[2], and I. Kadashevich[1]

1) Particle Technology, Nanostructured Materials, DelftChemTech, TUDelft, Julianalaan 136, 2628 BL Delft, The Netherlands.

2) Faculty of Aerospace Engineering, Kluyverweg 1, 2629 HS, Delft, The Netherlands.

Corresponding authors e-mail: s.luding@tudelft.nl

ABSTRACT

The self-healing behaviour of materials with a particulate microstructure, which has experienced damage under uniaxial compression or tension, is studied with the Discrete Element Method. The stress-strain response of the particle system shows that the effective compressive and tensile strengths typically increase with the contact adhesion (i.e., the tensile strength between particles), where the effective compressive strength is about 5 times larger than the tensile strength. A sample with "weak" contact adhesion is self-healed by instantaneously increasing the contact adhesion at different deformation levels from weak to "strong". The stress-strain curves of self-healed samples are bounded by an envelope curve that reflects the damage response of a sample that has a "strong" contact adhesion since the onset of loading. If self-healing is applied short before the peak stress is reached, the maximum sample strength will be close to maximum strength observed in the envelope curve. In contrast, if self-healing is initiated in the tensile softening regime, the maximum sample strength will be (significantly) less than the maximum strength related to the envelope curve.

Introduction

DEM modeling of particle systems

Discrete Element Method (DEM) studies on (thermo-)mechanical processes in particle systems illustrate that the effective response of these materials is characterized by various macroscopic properties, such as cohesion, friction, yield strength, dilatancy, stiffness, and anisotropy (Herrmann *et al.*, 1998; Vermeer *et al.*, 2001, Luding and Herrmann, 2001; Luding, 2004; Suiker and Fleck, 2004; David *et al.*, 2005; Luding 2005b). The macroscopic properties generally do not remain constant during the loading process, but depend on the actual deformation and/or temperature levels applied; for example, in a sintering process the adhesion between particles may strongly increase with temperature or pressure (Luding 2005, Luding 2007). In dynamic processes the effective response of particulate materials commonly can change rapidly with time, and therefore is more difficult to interpret than in quasi-static processes, especially if it originates from complex contact mechanisms (Mouraille *et al.*, 2006). Insight into the macroscopic behaviour can be improved through establishing direct links with the microstructural characteristics of the particulate material, i.e., micro-macro scale

transitions (Vermeer *et al.*, 2001; Suiker and Fleck, 2004; Luding, 2005b). Within the context of DEM modeling, such scale transitions can be achieved by first solving the equations of motion at the particle level, in a similar fashion as in the classical molecular dynamics approach (Allen and Tildesley, 1987). Subsequently, the effective response of the particle system (e.g., expressed in terms of stress and strain) is derived through averaging the local variables at the particle level (e.g., force and displacement) over the assembly volume. Provided that the particle shape is appropriately represented in the DEM model, the accuracy of the effective response solely depends on the chosen particle contact model (Tomas, 2001, Luding, 2001, Luding, 2006, Luding, 2007). This makes the approach very suitable for accurately predicting experimental results in a relatively straightforward fashion, and judging the validity of macroscopic constitutive models (Suiker and Fleck, 2004, Thornton and Zhang, 2006). In addition, a simple approximation of a system of complex-shaped particles by an assembly of spherical grains typically reproduces the qualitative response of the system rather well, even under fairly complicated loading paths (Thornton and Anthony, 2000), although recent studies have demonstrated that the accurate simulation of systems composed of non-spherical particles is possible as well (d'Addetta *et al.*, 2006).

Self-healing processes in particle systems

In the present study, it is anticipated that particle systems can be equipped with specific micromechanical healing characteristics, such that they are able to efficiently reduce, or even reverse, damage development caused by external loading. The self-healing capacity of particulate materials is analyzed using DEM modeling. Particle structures consisting of spheres with a cohesive-frictional contact law are studied under quasi-static monotonic uniaxial loading. The self-healing capacity of the particulate sample is simulated by instantaneously changing the contact adhesion (i.e., tensile contact strength between particles) at a specific deformation level. The main purpose of this study is to provide insight into how the strength and lifetime of the particulate sample can be efficiently enlarged.

Simulation Method

DEM studies are commonly performed on relatively small representative volume elements, where the number of particles is chosen such that the computational time of the simulation remains manageable. The purpose of such simulations is to achieve detailed insight into the kinematical and dynamical behaviour of the particles, and to relate this information to the effective mechanical properties of the sample. From the viewpoint of computational efficiency the incremental timestep used in the DEM simulations should be as large as possible; however, in practice, the magnitude of the timestep is limited by numerical stability requirements. The *critical timestep* for numerical stability can be estimated from the response period of a linear spring-dashpot model subjected to an initial displacement (Herrman *et al.*, 1998; Luding, 2007). In the present study the

integration timestep is chosen about 100 times smaller than this response period, which warrants the stability of the numerical procedure under arbitrary loading conditions and deformation paths.

Particle contact model

The non-linear contact model used is sketched in Fig. 1. The *normal contact force* f between two particles is governed by the normal contact overlap $\delta > 0$. During the initial compressive loading stage, the contact force increases proportionally with the contact overlap as $f = k_1 \delta$, where k_1 is the elasto-plastic contact stiffness. At a specific maximum contact overlap δ_{max}, the contact stiffness increases instantaneously to a value k_2. Loading and elastic unloading at this stage are prescribed in accordance with $f = k_2(\delta - \delta_f)$. Elastic unloading to a zero contact force leads to a contact overlap equal to the maximum plastic contact indentation, $\delta = \delta_f$. Further unloading brings the contact force in the tensile regime, where the maximum tensile contact force $f_{t,max}$ corresponds to a contact overlap $\delta = \delta_{t,max}$. Elastic unloading at a contact overlap smaller than δ_{max} occurs in accordance with a contact stiffness k_* that follows from a linear interpolation between the values k_1 and k_2. Additionally, the line $-k_t \delta$ characterizes tensile failure (i.e., softening), where the maximum tensile contact force is computed as $f_{t,max} = -k_t \delta_{t,max}$. For the sake of brevity, the tensile softening parameter k_t hereafter is referred to as the "contact adhesion".
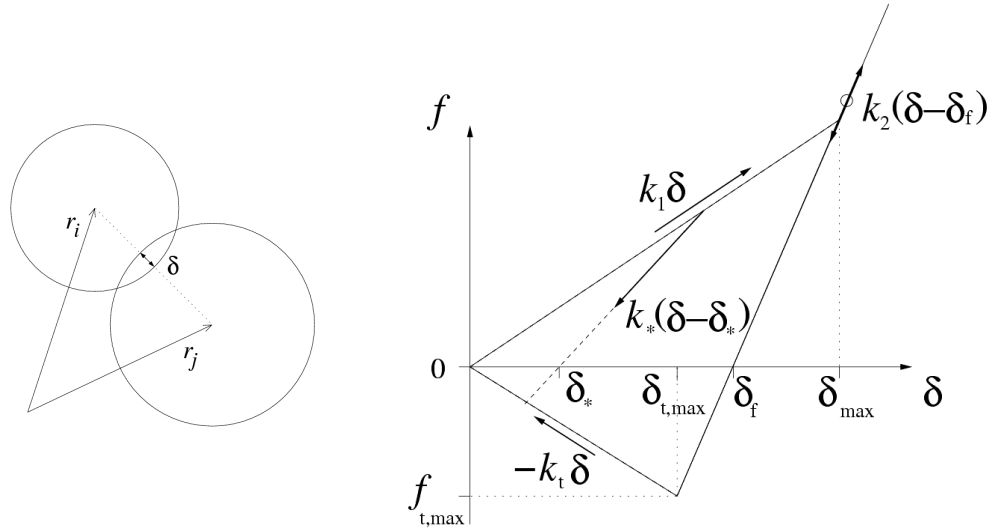

Fig. 1 (Left) Two-particle contact with contact overlap δ. (Right) Particle contact model in terms of the normal contact force plotted against the contact overlap (compression is assumed positive). For more details, see Luding (2005, 2006, 2007).

The *tangential contact force* parallel to the particle contact plane is related to the tangential contact displacement by means of a linear elastic contact law, with the tangential stiffness equal to k_s. The tangential contact displacement depends on both the translations and rotations of the contacting particles. A Coulomb friction law determines the maximum value of the tangential contact force: During sliding the ratio between the tangential contact force and the normal contact force is assumed to be constant and equal to the friction coefficient μ. In a similar fashion,

the elastic contact behaviour related to rolling and twisting (torsion) is set by the elastic constants k_r and k_o, respectively. The maximum values of the corresponding contact torques depend on the normal contact force through a Coulomb-type law with "friction" coefficients μ_r and μ_o, respectively. More details on the contact model can be found in Luding (2006, 2007).

The overall solution of the present non-linear DEM problem is obtained by integrating Newton's equations of motion for the translational and rotational particle degrees of freedom. In the case of short-range particle interactions, which are present in particulate media such as powders and sands, a considerable increase in computational time can be achieved by using a linked-cell method that allows for a more efficient particle neighborhood search. Hence, this procedure is applied for the present simulations, and more details on the algorithm can be found in Allen and Tildesley (1987).

System parameters and sample preparation

Material parameters and loading conditions

The simulations discussed in this section refer to a sample of 1728 poly-dispersed, spherical particles. The radii R_i of the particles are drawn from a Gaussian distribution around a mean value $\overline{R}$ = 0.005 mm (David *et al.*, 2005, Luding, 2007). Six outer walls forming a cuboidal volume with side lengths of 0.115 mm prescribe the geometry of the sample.

A loose assembly of particles is first subjected to an *isotropic pressure sintering* process (as detailed below) in order to obtain a sample that can be subjected to *uniaxial tension* or *uniaxial compression* loading. In the uniaxial compression tests, one of the two outer walls with its normal pointing in the axial (loading) direction is slowly moved towards the opposite wall. The change of the wall displacement in time is prescribed by a cosine function, which has a relatively large period in order to reduce inertia effects (Luding and Herrmann, 2001, Luding, 2004, Luding, 2005b). Uniaxial tension is applied in a similar fashion as uniaxial compression, i.e., one of the two outer walls with its normal pointing in the loading direction is moved away from the opposite wall.

The particle density is $\rho=2000$ kg/m^3. The maximum elastic contact stiffness is $k_2=5.10^4$ N/m, the elasto-plastic stiffness (expressed in terms of k_2) is $k_1/k_2=1/2$, and the tensile softening parameter k_t/k_2 is varied in the simulations. The maximum plastic contact indentation for two contacting particles with radii R_1 and R_2 is computed as $\delta_f = \phi_f\, 2R_1R_2/(R_1+R_2)$, with the maximum plastic indentation strain equal to $\phi_f = 0.05$.

The tangential stiffness, rolling stiffness and twisting stiffness have the values $k_s/k_2=1/5$, $k_r/k_2=1/10$, and $k_o/k_2=1/10$, respectively, and the friction coefficients corresponding to these deformation modes are $\mu=1.0$, $\mu_r=0.0$ and $\mu_o=0.0$. In order to limit the computational time necessary for reaching static equilibrium, the model is extended with viscous damping (i.e, the contact force related to damping is proportional to the contact velocity), with the damping coefficient in the normal direction being equal to $\gamma = 5$ kg/s, and the tangential damping, rolling damping

and twisting damping (expressed in the same units as the normal contact damping) equal to $\gamma_s / \gamma = 1/5$, $\gamma_r / \gamma = 1/10$, $\gamma_o / \gamma = 1/10$. In addition, translational and rotational background viscosities are introduced when computing the overall forces and torques acting on the individual particles. This is done in order to efficiently dissipate dynamic response contributions related to relatively long wavelengths. The values of the translational and rotational background viscosities are $\gamma_b / \gamma = 1$ and $\gamma_{br} / \gamma = 4$, respectively. Additional computations not presented here, in which the loading rate was set a factor of two lower than in the present simulations, have confirmed that the influence of the viscosity on the system response is minor; i.e., no considerable change in the peak strength was observed and the stress profile related to softening branch was altered only slightly. More details on the above material parameters can be found in Luding (2006, 2007).

The incremental timestep, which is chosen in accordance with the procedure mentioned previously, equals $\Delta t = 5.10^{-10}$ s. Additional computations not presented here have shown that an incremental timestep of two to three times larger than this value leads to spurious numerical results, whereas a two times smaller timestep changes the numerical results only minorly.

Preparation of the sample

As already mentioned, the sample is prepared through subjecting a loose assembly of particles to a *pressure sintering* process. Accordingly, a hydrostatic pressure $p_s / \sigma_0 = 10^{-2}$ (with the reference stress $\sigma_0 = k_2/\overline{R}$, where $\overline{R} = 0.005$ mm is the average particle radius) is applied by uniformly displacing the six outer walls such that the cuboidal sample decreases monotonically in volume. The contact surfaces between the particles deform plastically as a result of the relatively large value of p_s. During the sintering process the particle contacts are frictional (in correspondence with the friction coefficients mentioned above), while the walls are virtually frictionless ($\mu_{wall} = 0.01$). The contact adhesion is set to zero ($k_t/k_2 = 0$) for all particle-wall contacts, except for the particle-wall contacts in the loading direction, for which high values of $k_t/k_2 = 20$ are used in order to warrant that these particles directly follow the uniaxial tensile loading applied later. The other contact parameters have the same values as mentioned above. The hydrostatic loading process is considered to be finished when the kinetic energy of the sample is negligible compared to the potential energy. During sintering the value of the adhesion hardly affects the response, since most particles are loaded in compression; additional computations not presented here showed that virtually identical results are obtained for contact adhesion values in the range $0 < k_t/k_2 < 0.5$. The solid volume fraction obtained after pressure sintering is $\nu = 0.676$ (which relates to a porosity of $1 - \nu = 0.324$), and the average coordination number is $C = 7.17$.

Upon subsequent *stress relaxation*, the contact adhesion between the particles is increased to $k_t/k_2 = 1/5$, and the external hydrostatic pressure is reduced to virtually zero, $p_s / \sigma_0 = 10^{-5}$. Due to the presence of a tensile strength between the particles, the lateral stability of the specimen remains preserved when the hydrostatic pressure is released. The solid volume fraction after stress relaxation is $\nu = 0.63$ and the coordination number is $C = 6.09$.

Results

Failure under uniaxial compression and uniaxial tension

The responses of the sample under uniaxial compression and uniaxial tension are shown in Fig. 2 (Left). The normal axial stress σ (normalized by the reference stress $\sigma_0 = k_2/\overline{R}$) is plotted as a function of the normal axial strain ε (where positive stress and strain values relate to compression). The stress-strain curves are depicted for different values of k_t (normalized by k_2), which quantifies the adhesion at the particle contacts, see Fig. 1. Both under uniaxial tension and uniaxial compression a larger adhesion increases the effective strength of the sample. Furthermore, the overall strain at which the effective stress reaches its maximum increases with an increasing value of k_t. The maximum stress under compression is about 5 times larger than under tension. In addition, the softening branch under uniaxial tension is somewhat steeper than under uniaxial compression. The initial axial stiffness in tension and compression, which is determined by the sample preparation procedure, is approximately equal for all cases considered here, and corresponds to a (normalized) value of $C_t / \sigma_0 = 0.26$. All tensile responses plotted in Fig. 2 (Right) relate to a local failure pattern at the center of the sample. However, additional simulations not presented here have shown that local failure may also occur nearby one of the outer walls in the axial direction if the particle adhesion is equal or higher than the value of $k_t/k_2=20$ used for the walls. In addition, changing the rolling and twisting frictions from $\mu_r =\mu_o=0.0$ to $\mu_r =\mu_o=0.2$ increased the tensile peak strength of the sample with about 20%, and a further increase of these friction parameters only minorly changed the stress-strain responses.
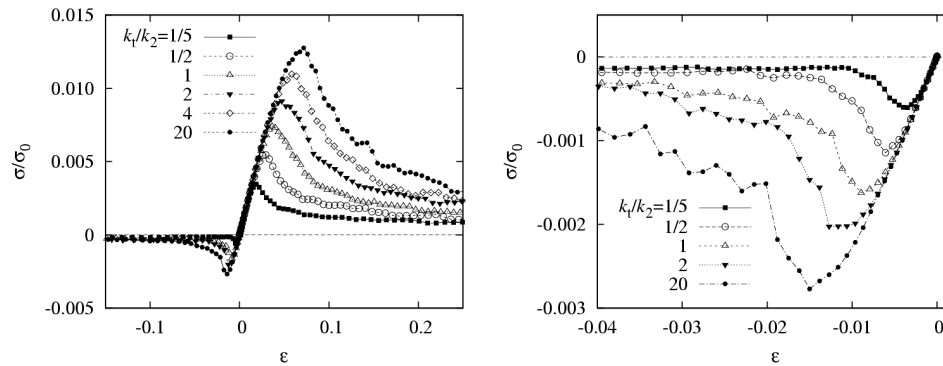

Fig. 2 (Left) Axial stress versus axial strain during uniaxial compression (positive stress and strain values) and uniaxial tension (negative stress and strain values), for different particle contact adhesions k_t (normalized by k_2). (Right) Magnification of the tensile responses plotted in the left figure.

Self-healing under uniaxial compression

Under uniaxial compression the self-healing behaviour of a relatively weak sample with $k_t/k_2 = 1/5$ is simulated by instantaneously increasing the contact

adhesion to $k_t/k_2 = 1$. This self-healing mechanism is assumed to take place at all particle contacts, and is studied by initiating it at different deformation levels. Fig. 3 shows several self-healing response curves (dashed lines, labeled with the abbreviation SH), together with the stress-strain responses of the "weak" ($k_t/k_2 = 1/5$, solid squares) and "strong" ($k_t/k_2 = 1$, triangles) samples, taken from Figure 2. It is observed that the maximum compressive strength reached during self-healing is larger when self-healing is initiated at smaller axial strain. Hence, from the aspect of strength optimization, during the deformation process the self-healing mechanism should be activated relatively early. Furthermore, for all self-healing cases considered the response eventually converges with the damage response of the "strong" sample with $k_t/k_2 = 1$. This is expected, since the damage response of the strong sample may be interpreted as a "self-healing" response with the increase in contact adhesion to $k_t/k_2 = 1$ initiated at the onset of the loading process. Consequently, the damage response for $k_t/k_2 = 1$ acts as an envelope for the self-healing responses with k_t/k_2 increased from $1/5$ to 1 at arbitrary deformation levels.
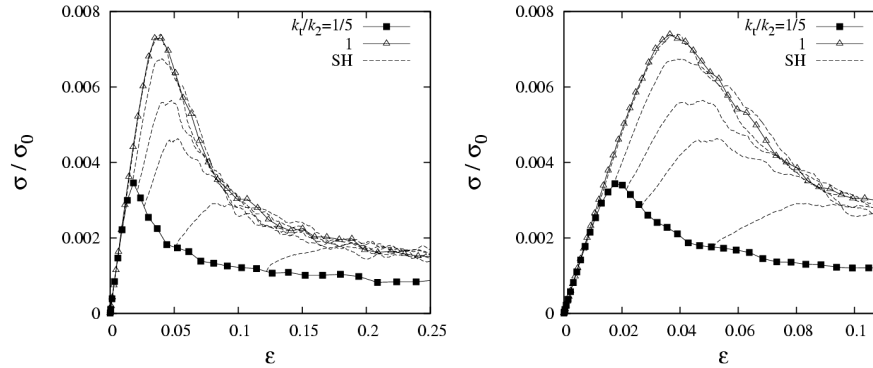

Fig. 3 (Left) Axial stress versus axial strain during uniaxial compression. The lines with solid squares and open triangles represent the damage responses of the weak ($k_t/k_2=1/5$) and strong ($k_t/k_2=1$) samples, respectively, as taken from Fig. 2. The dashed lines reflect the responses after the initiation of self-healing (which occurs by increasing the contact adhesion to $k_t k_2=1$) at various deformation levels. (Right) Magnification of the responses plotted in the left figure; the initiation of self-healing occurs at axial strains $\varepsilon \approx 0.016, 0.019, 0.022, 0.026, 0.045,$ and 0.12.

Self-healing under uniaxial tension

In the case of uniaxial tension, self-healing is investigated by increasing the contact adhesion at different deformation levels from $k_t/k_2 = 1/5$ to $k_t/k_2 = 1$ (Fig. 4, Left) and to $k_t/k_2 = 20$ (Fig. 4, Right). Similar to the self-healing responses under uniaxial compression plotted in Fig. 3, the maximum tensile strength of the healed sample is larger if healing is initiated at an earlier deformation stage. Further, the responses of the healed samples eventually coincide with the damage responses of the strong samples with $k_t/k_2 = 1$ (Fig. 4, Left) and the very strong sample with $k_t/k_2 = 20$ (Fig. 4, Right). A comparison between self-healing curves in Figs. 4 (Left) and (Right) shows that a stronger increase in contact adhesion clearly gives rise to a larger sample strength.
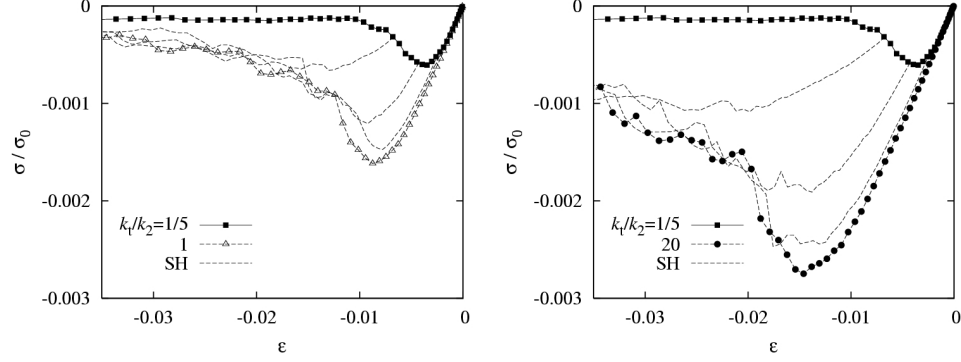
Fig. 4 Axial stress versus axial strain during uniaxial tension. The lines with solid squares, open triangles, and solid circles represent the damage responses of the weak ($k_t/k_2=1/5$), strong ($k_t/k_2=1$) and very strong ($k_c/k_2=20$) samples, respectively, as taken from Fig. 2. The dashed lines reflect the responses after the initiation of self-healing, which occurs by increasing the contact adhesion to $k_t/k_2=1$ (Left) and $k_t/k_2=20$ (Right) at various deformation levels ($\varepsilon \approx -0.005$, -0.006 and -0.007).

Concluding remarks

Self-healing processes in damaged, adhesive particulate materials have been studied under uniaxial compression and uniaxial tension using DEM simulations. The self-healing mechanism is initiated at the particle contact level by instantaneously increasing the contact adhesion from "weak" to "strong". The stress-strain responses under self-healing eventually converge to the envelope curve that represents the damage response of a particulate sample that has the same strong contact adhesion since the onset of loading. This behaviour is independent of the overall deformation level at which the self-healing mechanism is activated. Nonetheless, the maximum sample strength reached during self-healing very much depends on the deformation level at which self-healing is activated: If self-healing is activated short before the peak-stress is reached, the maximum sample strength will be close to peak strength observed in the envelope curve. In contrast, if healing is initiated in the softening regime, the maximum sample strength may be considerably less than the maximum strength related to the envelope curve.

In the present study the self-healing mechanism was instantaneously initiated at *all* particle contacts in the sample. However, it is energetically favourable to activate self-healing at a relatively early stage in the loading process, which requires an early identification of local damage development in a sample. Also, to improve the efficiency of the healing process, only those parts of the sample should be healed for which the damage has surpassed a specific critical level. Furthermore, it is more realistic to initiate the self-healing mechanism over a specific period in time, instead of initiating it instantaneously. These are topics for future numerical studies, where the results of these studies (and the present study) require an experimental validation.

8

ACKNOWLEDGEMENTS

REFERENCES

Allen M. P. & Tildesley D. J., (1987), Computer simulation of liquids, Oxford University Press Inc., New York.

D'Addetta, G. A., Kun, F., Ramm, E., (2002) On the application of a discrete model to the fracture process of cohesive granular materials, *Granular Matter* **4** (2), 77-90.

David, C. T., Garcia-Rojo, R., Hermann, H. J., and Luding, S. (2005), *Hysteresis and Creep in Powders and Grains*, in: Powders and Grains 2005, R. Garcia Rojo, S. McNamara, and H. J. Herrmann (Eds.), Balkema.

Herrmann, H. J., Hovi, J.-P., and Luding, S., (Eds.) (1998) *Physics of dry granular media*, NATO ASI Series E 350, Kluwer Academic Publishers, Dordrecht, Netherlands.

Luding, S., and Herrmann, H. J. (2001), *Micro-Macro Transition for Cohesive Granular Media*, in: Zur Beschreibung komplexen Materialverhaltens, Institut für Mechanik, S. Diebels (Ed.), Stuttgart, pp 121-134.

Luding, S. (2004), Micro-macro transition for anisotropic, frictional granular packings. *International Journal of Solids and Structures* **41**, 5821-5836.

Luding, S., Manetsberger, K., and Muellers, J. (2005), A discrete model for long time sintering, *Journal of the Mechanics and Physics of Solids* **53**(2), 455-491.

Luding, S. (2005), Granular Media – Information propagation. *Nature* **435** (7039) 159.

Luding, S. (2005b), Anisotropy in cohesive, frictional granular media, *Journal of Physics: Condensed Matter* **17**, S2623-S2640.

Luding, S. (2006), *About contact force-laws for cohesive frictional materials in 2D and 3D*, in: Behavior of Granular Media, P. Walzel, S. Linz, Ch. Krülle, and R. Grochowski (Eds.), Band 9, Schriftenreihe Mechanische Verfahrenstechnik, ISBN 3-8322-5524-9, Shaker Verlag, Aachen 2006, pp. 137-147.

Luding, S. (2007), Tensile tests with new contact laws for frictional granular particles. *Granular Matter* (submitted).

Mouraille, O., Mulder, W. A., Luding, S. (2006), Sound wave acceleration in granular materials. *Journal of Statistical Mechanics- Theory and Experiment*, P07023.

Suiker, A. S. J. and Fleck, N.A., (2004). Frictional collapse of granular assemblies. *Journal of Applied Mechanics* **71**, pp. 350-358.

Thornton, C., and Antony, S. J. (2000), Quasi-static deformation of a soft particle system, *Powder Technology* **109**(1-3), 179-191.

Thornton, C., and Zhang, L. (2006), A numerical examination of shear banding and simple shear non-coaxial flow rules, *Philosophical Magazine* **86**(21-22), 3425-3452.

Tomas, J. (2001), Assessment of mechanical properties of cohesive particulate solids – part 1: particle contact constitutive model, *Particle Science Technology* **19**, 95-110.

Vermeer, P. A., Diebels, S., Ehlers, W., Herrmann, H. J., Luding, S., and Ramm, E., eds., *Continuous and Discontinuous Modelling of Cohesive Frictional Materials*, Lecture Notes in Physics 568, Springer, Berlin, 2001.